Journal of New Technology and Materials
JNTM
Vol. 02, N°01 (2012)17-21

OEB Univ. Publish. Co.

# The electrochemical nucleation and properties of the Co-Cu alloys thin films deposited on FTO substrate

L. Mentar* and A. Azizi
*Laboratoire de Chimie, Ingénierie Moléculaire et Nanostructures, Département de Chimie, Faculté des Sciences, Université Ferhat Abbas- Sétif, 19000 Algérie*
*menter.loubna@yahoo.fr
*Received: Jan 20, 2012; revised: March 14, 2012; accepted: March 28, 2012*

**Abstract**
*In this study, the properties of Co-Cu alloys thin films prepared by the electrodeposition method from a sulfate bath under potentiostatic conditions on a fluorine-doped tin oxide (FTO)-coated conducting glass substrate have been investigated. The electrochemical characteristics of granular alloys were studied by using cyclic voltammetry (CV) and chronoamperometry (CA) techniques. The structural behaviors of the deposits have been determined by X-ray diffraction (XRD) measurements. The magnetic properties were investigated by alternating gradient force magnetometer (AGFM) technique. The effect of deposition potential on the electrodeposition process, phase structure and magnetic behaviors has been studied. CV studies revealed that the potential of Co dissolution depends on experimental parameters such as presence of Cu ions and cathodic limit. X-ray diffraction patterns of the Co-Cu alloys thin films exhibit an fcc and hcp phases, with peaks quite close to those of the Co phase (fcc and hcp). Magnetic properties such as coercivity and saturation magnetization showed strong dependence on the crystallite size and consequently the deposition potentials.*
***Keywords** : electrodeposition; Co-Cu alloys; structure; magnetic.*

## 1. Introduction

Systems, composed of immiscible materials such as Co-Ag or Co-Cu [1, 2] consist of small grains of the magnetic metal isolated in the non-magnetic matrix. The difference in the spin-dependent scattering for aligned and randomly oriented magnetic moment generates a giant magnetoresistance (GMR). The discovery of this phenomenon in Co-Cu systems, thin films of cobalt and copper has been investigated for basic research and applications [3]. The effect is exploited commercially by manufacturers of hard disk drives, the magnetic sensors on the reading heads of computers or some music players, etc. The granular alloy films are immiscible combinations usually prepared by physical deposition methods [1,4]. Recently, electrochemical deposition is widely used to produce multilayered alloys exhibiting giant magnetoresistance (GMR) [5-16]. This technique is preferred in low-end applications such as GMR sensors in automotive applications or in microsystems [15, 16]. The simplicity, cost effectiveness, easy scale up, and possibility to grow films on irregular surfaces make the process more versatile. The solid solubility limit of Cu in Co at room temperature is almost 0% in the equilibrium state [17]. However, the electrodeposition made the Co-Cu alloy in nonequilibrium supersaturated solid solution state. It is well known, that the nucleation-growth process, the morphology, the microstructures and magnetic properties of Co-Cu electrodeposits depend greatly on solution composition, pH, temperature, and applied potential or current density [18-27]. Several baths with different compositions have been used for electrodeposition of Co-Cu thin films. Among them the bath, with or without additives, are usually used to electrodeposite Co-Cu granular thin films. The formation of continuous film of Co-Cu alloys thin films requires a detailed understanding of the microstructure and the role of parameters such as applied potential on the properties of deposits. Consequently, the aim of this work is to study of the influence of the deposition potential in the electrochemical nucleation and the properties of the Co-Cu alloys thin films. The electrochemical behaviour and composition of the deposited alloys were analyzed as a function of the applied potential. X-ray diffraction (XRD) and alternating gradient force magnetometer (AGFM) analysis were carried out on some deposits obtained potentiostatically.

## 2. Experimental Details

Co-Cu thin films were prepared by electrodeposition onto polycrystalline fluorine-doped tin oxide (FTO)-coated conducting glass substrate with an exposed area of $1\times2$ $cm^2$ ($10-20$ $\Omega/cm^2$ sheet resistance). All the depositions were made in a three-electrode cell containing Pt as a counter electrode, saturated calomel electrode (SCE) as reference and FTO coated glass as a working electrode. The FTO substrate was first degreased in acetone and ethanol by ultrasonication for 15 min, and lastly well rinsed with distilled water. The thin films alloys were deposited in a potentiostatic mode, using a computer controlled potentiostat/galvanostat (Voltalab 40) as a potential source. The electrolyte contained 0.25M cobalt sulfate, 0.005 M copper sulfate, 1M sodium sulfate, and 0.5M boric acid, pH was adjusted to 3.8 using diluted $H_2SO_4$. Electrodeposition was performed at room temperature, without stirring. The structural characterization was performed by XRD through θ-2θ scans using a Siemens D5000 diffractometer equipped with a monochromatic Cu source ($\lambda CuK\alpha_1$ = 0.154056 nm). The magnetic measurements were performed with an alternating gradient force magnetometer (AGFM) at room temperature.

## 3. Results

To define the major characteristics of the Cu, Co and Co-Cu alloy deposition process, the cyclic voltammetry technique was used. Typical CVs of FTO electrode recorded in (a) 0.25

M $CoSO_4$ and (b) 0.25 M $CoSO_4$ + 0.005 M Cu $SO_4$ solutions are shown in Fig. 1. On the forward scan, the voltammograms show an abrupt increase in current at a potential of approximately −1.03 V vs. SCE which is the starting point of the reduction of the Co species. Fig. 1a also shows that dissolution of the deposits starts at around 0.0 V on the reverse scan, in agreement with previous studies on the electrochemical deposition of $Co^{2+}$ onto FTO electrodes in sulfate aqueous solutions [28]. Figure 1b shows the CV of the 0.25 M $CoSO_4$ + 0.005 M $CuSO_4$ solution. In the direct scan, the beginning of the current decrease was detected at -0.14 V vs. SCE, which is characteristic of the overpotential deposition process of Cu onto FTO surfaces [29]. After this of Cu onto FTO, the Co deposition on Cu surface starts at around -0.89 V vs. SCE. In this case, the Co deposition potential value shifts anodic than that Co free solution. It's well established that the over-potential of metal deposition on foreign substrate is high than deposition on metal substrate. In effect, in the negative scan, Co deposited on Cu deposits instead of the FTO surface because Cu deposited at much lower negative potential than Co and the electrode surface was covered by Cu deposits before Co deposited. Since Co and Cu have very similar crystallographic structure, lower energy is required by Co to nucleate on Cu [30]. Therefore, the nucleation potential of Co shifted positive slightly, from −1.03 to -0.89 V vs.SCE, in the presence of Cu ions. On the reverse scan at -1.3 V; an intense anodic peak are observed comparable to that observed during the Co dissolution (Fig. 1a). This intense peak corresponds to Co-rich phases. Since Co and Cu could form alloy or intermetallic compounds from Co-Cu phase diagram, this peak attributed to Co-Cu phase is very rich in Co due to the very lower $Cu^{2+}$ concentration in solution. This behavior is in agreement with the literature [30, 31]. In addition, the increase or decrease of dissolution peaks can be related to the composition of the dissolved deposit. On the other hand, the presence a crossover occurred between the cathodic and anodic current branches is the sign of a nucleation and growth process [31].

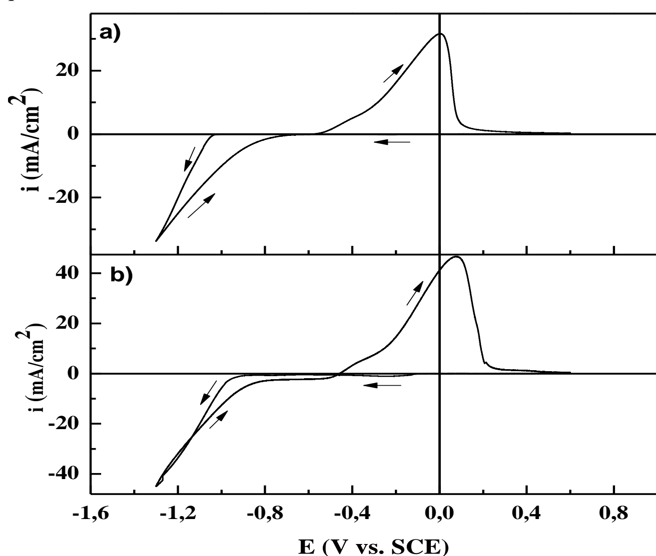


**Figure 1** Cyclic voltammogram of FTO substrate in (a) 0.25 M $CoSO_4 7H_2O$ and (b) 0.25 M $CoSO_4 7H_2O$ + 0.005 M $CuSO_4 7H_2O$ with 1 M $Na_2SO_4$ and 0.5 M $H_3BO_3$ (pH=3.8) solutions. v= 20 $mVs^{-1}$.

To confirm the precedent cyclic voltammetry study, the Figure 2 presents the voltammograms obtained from a solution with Co and Cu ions at different switching potentials ($E_\lambda$). $E_\lambda$ values were chosen to be within the zone where the reduction processes are observed in the voltammograms. The number of anodic peaks is related to the switching potentials. Effectively, only one peak $A_2$ is observed at -0.7 and -0.9 V vs. SCE. The position of this peak is related to dissolution of copper [29]. Moreover at -1.0 and -1.1 V vs. SCE, two anodic peaks $A_1$ and $A_2$ are observed. By comparing this cyclic voltammetric curves with of the oxidation of pure cobalt shown in Fig. 1a, it could be concluded that peak $A_1$ corresponding to the cobalt oxidation. At higher applied potential, -1.2 and -1.3 V, only one higher peak is observed ($A_3$), which could be attributed to Co-Cu phase very rich in Co. this can be related to decrease in copper (II) ions concentration in the solution.

In all cases, the anodic peaks shifted slightly in the positive direction. The cathodic and anodic current density increased with increasing value of switching potential, which indicated that more Co deposits were obtained in the cathodic region with a higher negative applied potential. Adjustment of the applied current led to the preparation of Co-Cu films with variable metal percentages. It was also found (see Fig. 2) that the ratio of the peak area $A_1$ to total anodic peak became smaller when higher negative switching potential was applied, which indicated that the copper percentage in the deposits was reduced with the higher negative electrodeposition potential applied. These results corroborate the voltammetric deposition curves, (Fig. 2b), i.e., these curves were similar to those obtained in the literature [32, 35]. The increase in polarization with increasing Co concentration in Co-Cu deposits is reported in these references. Also, this is confirmed by elemental composition of granular alloys deposited at different applied potential realized using the atomic absorption spectroscopy (AAS) measurements (not shown).

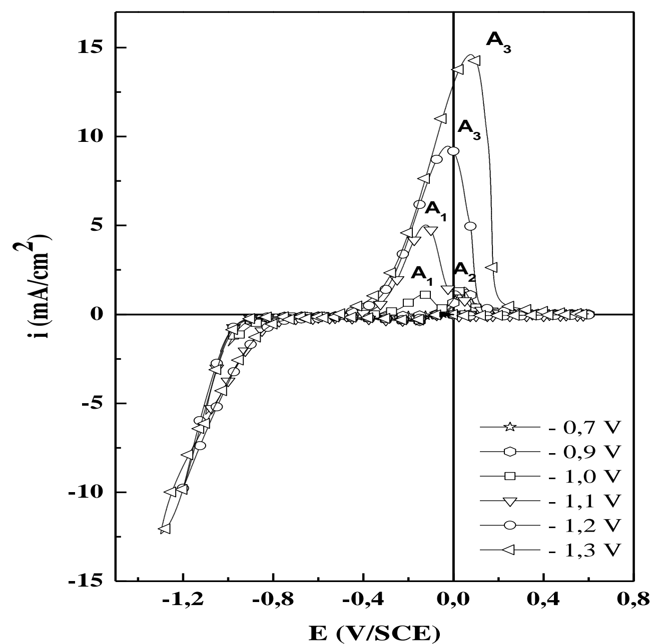


**Figure 2** Voltammetric curves of Co-Cu alloy deposition and dissolution from electrolytic solution 0.25 M $CoSO_4 7H_2O$ + 0.005 M $CuSO_4 7H_2O$ and 1 M $Na_2SO_4$ and 0.5 M $H_3BO_3$ (pH=3.8) solutions with six different cathodic sweep reversal potentials: from -0.7 V to -1.3 V; v = 20 mV $s^{-1}$

The nucleation kinetics and growth of Co-Cu onto FTO surface was studied with the chronoamperometry technique. This technique is frequently used to determine the mechanisms by which new phases are formed. The formation

of stable nuclei and their growth can be observed by monitoring the current and information on the rate of nucleation, the density of nuclei and the mechanism of growth can be obtained from the shape of the resulting current–time transient plots [29]. An example of current transients obtained at different potentials during Co-Cu electrodeposition on FTO coated glass substrates are shown in Fig. 3. It can be seen that all the curves have a characteristic peak corresponding to the nucleation of Co-Cu alloy on FTO substrate. For longer deposition time, the current density also exhibits an asymptotically decaying behavior after reaching its maximum. This asymptotic behavior of the current densities indicates a nucleation followed by diffusion controlled growth. Moreover, it is found that the current density reaches the maximum value more rapidly with increasing the potential and also increases monotonically with the potential.

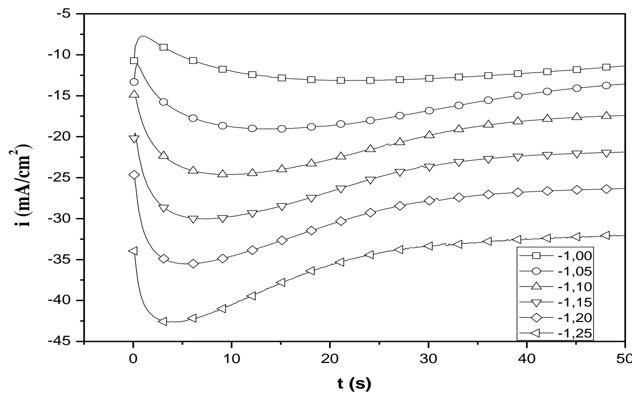


**Figure 3** Current transients for Co-Cu electrodeposition on FTO-coated conducting glass substrates at the indicated final potentials.

These features are qualitatively consistent with the theoretical 3D nucleation followed by diffusion controlled growth model suggested by Scharifker and Hills [33, 34]. According to this model, the nucleation is classified into two modes: the instantaneous nucleation and the progressive nucleation modes. In instantaneous nucleation mode, all reaction sites of the surface are activated simultaneously and the number of nuclei growing on the surface is saturated at the initial deposition stage. On the other hand, in progressive nucleation mode, the number of nuclei formed on the surface is less than the maximum saturation value and new nuclei begins to grow, progressively.

In order to distinguish between instantaneous and progressive nucleation process, experimental chronoamperometric data are used by representing in a nondimensional plot $\left(\frac{i}{i_{\max}}\right)^2$ versus $\left(\frac{t}{t_{\max}}\right)$ and to compare these with the theoretical plots resulting from the following equations:

-for instantaneous nucleation followed by three-dimensional diffusion-limited growth is:

$$\frac{i^2}{i^2_{max}} = \frac{1.9542}{t/t_{max}}\left\{1-exp\left[-1.2564\left(t/t_{max}\right)\right]\right\}^2 \quad (1)$$

- and for progressive nucleation followed by three-dimensional diffusion-limited growth is:

$$\frac{i^2}{i^2_{max}} = \frac{1.2254}{t/t_{max}}\left\{1-exp\left[-2.3367\left(t/t_{max}\right)^2\right]\right\}^2 \quad (2)$$

where i and t are the current density and time, respectively; $i_{max}$ and $t_{max}$ are maximums of the current transients and time, respectively. To analyze the experimental data by means of the theoretical model, the current transients in Fig. 3 are replaced with reduced-variable plots normalized in terms of imax and tmax. According to eqs. (1) and (2), these plots are presented in Fig. 4.

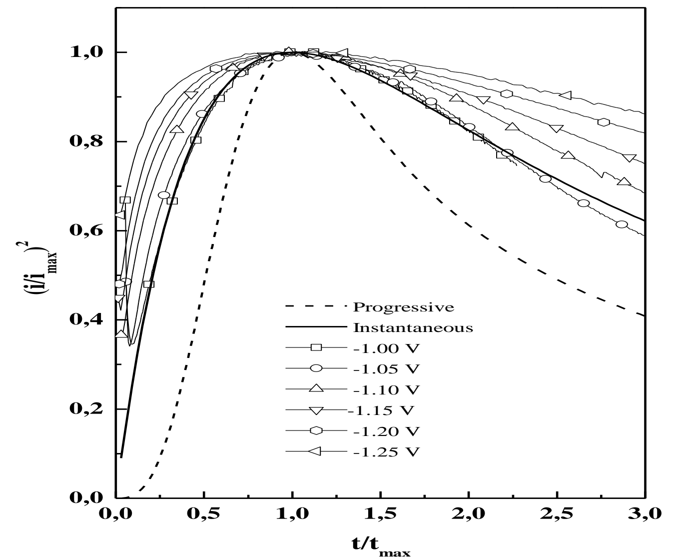


**Figure 4** Normalized$\left(i/_{i_{max}}\right)^2$ vs $\left(t/_{t_{max}}\right)$plots obtained from the experimental data in Fig. 3. The dotted and the solid line represent the theoretical progressive and instantaneous nucleation models, respectively.

The theoretical model curves are also shown in Fig. 4 and the solid line and the dotted line represent the theoretical plots with respect to instantaneous and progressive nucleation modes, respectively. It can be seen in the figure that all the experimental plots agree well with the instantaneous nucleation mode. This result indicates that in the initial deposition stage of Co-Cu on FTO surfaces, all the reaction sites on the surface of FTO substrate are activated simultaneously and the number of nuclei formed is saturated instantaneously.

The effect of electrodeposition potential on the phases formed in the Co–Cu thin films was analyzed using XRD. Fig. 5 shows the XRD patterns of Co-Cu thin films deposited at various applied potentials. Four peaks at 2θ values of 41.7, 44.28, 47.6 and 51.50 deg corresponding to hcp Co (100), (fcc Co (111), hcp Co(101) and fcc Co(201) planes of Co were observed, respectively. Furthermore these patterns display an fcc and hcp phase, with peaks quite close to those of the Co phase (fcc and hcp). No peaks of the Cu fcc pahse were found, which we suggest is due to the Cu clusters being too small to produce reflections [35] and only produce a distorsion of the Co lattice. It is interesting to note that such a distinct phase separation was not observed in the X-ray diffractogram studied by most of the previous researcher's [23, 25, 32] under DC deposition of Cu-Co alloys from an electrolyte without additive agent, except studies by Cohen-Hyams et al. [26]. Indeed, the annealing at high temperatures was found to improve such phase segregation in Cu–Co alloys.

From these results, it's evident that the fcc phase is dominant than the hcp phase in the Co-Cu alloy thin films. Apparently, the amount of the hcp phase increases when the applied potential decreases down to more negative value.

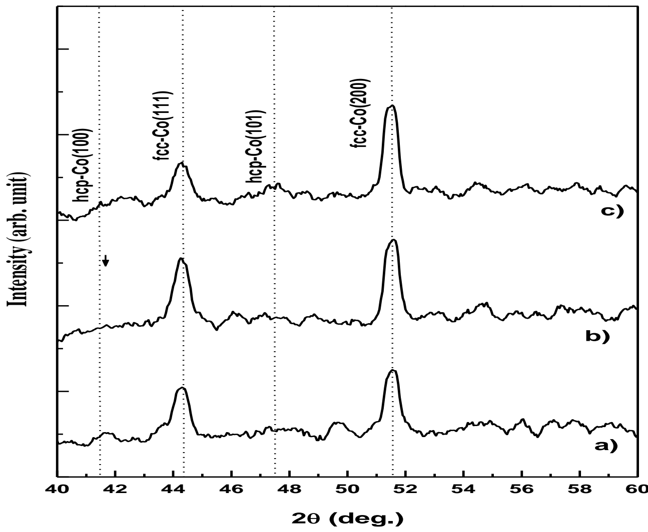


**Figure 5** XRD patterns of Co-Cu thin films deposited at various applied potentials: a) – 1.1, b) -1.2 and c) -1.3 V vs. SCE, respectively.

These results are in agreement with other observations [25]. For the all granular coating of Fig. 5, the adjustment of the average cell parameters led to an '*a*' value of 0.35402 nm, this value is slightly smaller than that of pure fcc Co, 0.35446 nm (JCPDS No. 15-806), which can be explained by strains induced by the presence of Cu and fcc Co in the matrix. Under equilibrium conditions, at room temperature the Co metal exists in the hcp phase, though the fcc phase is stable above 420°C only [36]. It is known that electrochemical deposition from a bath at pH more than 2.9 results mainly in an hcp-Co [37, 38]. However, in the literature the formation of fcc-Co phase by electrodeposition at room temperature is due the presence of codischarged and dissolved hydrogen distorting the hcp lattice to an extent that it finally transformed to the fcc structure [39]. Moreover, it has been shown that when the electrolyte has pH value about 3, and in the absence of stirring, the fcc structure is favored [40]. In this case for Co-Cu electrodeposited at more negative potential, the origin for the formation of an alloy with fcc phase was due to the incorporation of a very small impurity of Cu atom in the deposit [41].

The average crystallite size along the (111) peak for fcc phases estimated from the full width at half-maximum (FWHM) values of diffraction peaks using the Scherrer formula [42],

$$D=\frac{0.9\lambda}{\beta\cos\theta} \quad (3)$$

where $D$ is the crystallite size, $\beta$ is the broadening of the diffraction line measured at half of its maximum intensity in radiance (FWHM), $\lambda$ is the x-ray wavelength (1.5406 A°) used and $\theta$ is the diffraction angle. In table 1, the average crystallite sizes along the (111) peak for fcc phases at different values of applied potential are presented. The crystallite size was typically 20-40 nm. The alloy deposits therefore possess a nanocrystalline structure.

| E (V vs. SCE) | $2\theta$ (°) | D (nm) | $H_c$ (Oe) | Ms (emu/cm$^3$) |
|---|---|---|---|---|
| -1.1 | 44.31 | 40 | 25.80 | 1868.70 |
| -1.2 | 44.26 | 40 | 22.62 | 1408.61 |
| -1.3 | 44.32 | 21 | 64.52 | 547.24 |

Table 1: The effect of deposition potential on the structural and magnetic parameters of the Co-Cu alloy thin films.

Magnetization versus magnetic field curves (M vs. H) was registered in order to analyze the magnetic response for the deposits. Fig. 6 shows the hysteresis loops of the Co-Cu films at parallel and perpendicular to the film plane at room temperature obtained at three deposition potentials, (a) -1.1, (b) -1.2 and (c) -1.3 V vs. SCE, respectively. Also, table 1 summarizes the relevant magnetic properties. These results show change in the magnetic properties, which were related to the difference in grain sizes and thickness of deposit films. Magnetic anisotropy is clearly in plane and magnetization switches by domain-wall motion. The coercivity is small (24–70 Oe) and increases greatly as applied potentials increases from -1.1 to -1.3 V vs. SCE, indicating an increase in defect density when growth is made to occur faster. This is also verified by the XRD patterns in Fig. 5, where the diffraction peaks of the film grown at -1.3 V vs. SCE are much weaker than the other ones.

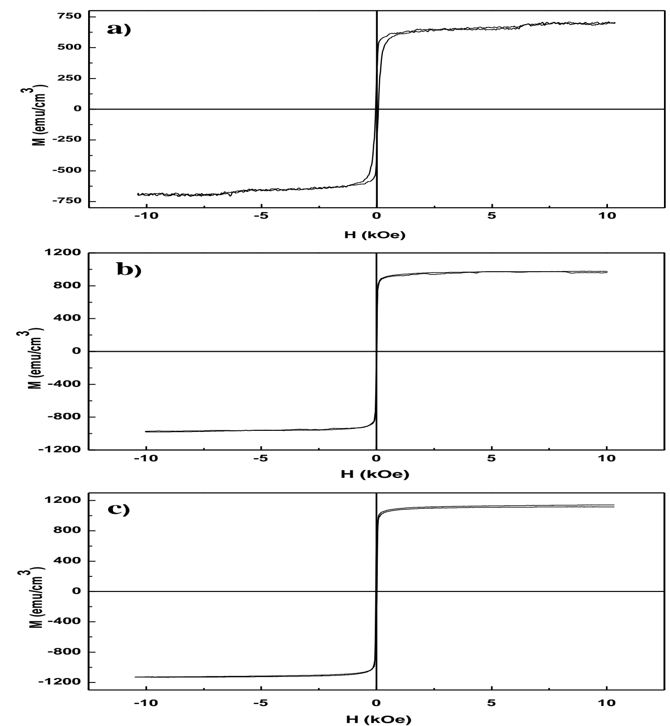


**Figure 6** Hysteresis loops of Co-Cu thin films along the easy and hard magnetized orientations obtained at different applied potential: (a) -1.1, (b) -1.2 and (c) -1.3 V vs. SCE, respectively.

## 4. Conclusion

In this work, electrochemical nucleation, structural and magnetic behaviors of cobalt–copper electrodeposits obtained from a free-sulfate bath with boric acid was investigated. The effect of deposition potential on the properties of Co-Cu alloys thin films has been investigated by means of cyclic voltammetry, chronoamperometry, XRD and AGFM techniques. The experimental results show that the composition of Co-Cu electrodeposits varied with the deposition potential and the mechanism for formation of deposit is preceded growth by 3D crystallites. The deposits formed from all deposition potential a weak crystallization state and showed a mixture of Co fcc and hcp phases structure. AGFM measurements indicate that the films grown obtained at all applied potential have in-plane magnetic anisotropy and small coercivity.

**References**

[1] AE. Berkovitch, JR. Mitchell, MJ. Carey, AP. Young, FE.Spade, FT. Parker, A.Htten , G. Thonaas, Phys. Rev. Lett. 68 (1992) 3745.

[2] J. Xiao, J. Jiang and C. Chien, Phys. Rev. Lett. 68 (1992) 3749; Phys. Rev. B 46 (1992) 9266.

[3] Y. Chen, Y. Mei, R. Kaltofen, J. I. Mönch, J. Schumann, J. Freudenberger, H. J. Klauß, and O. G. Schmidt, Adv. Mater. **20**, 3224 (2008).

[4]. J Q. Xiao, J S . Jiang , CL.Chien, ibid. 68 (1992) 3749.

[5] J . Yahalom, O. Zadok, J. Mater. Sci. 21 (1987) 499.

[6] H J. Blythe, VM. Fedosyuk, Phys. Stat. Sol. (a) 146 (1994) K13

[7] OF . Bakkaloglu, I H. Karahan, H. Efeoglu, M. Yildirim, U. Cevik , YK. Yogurtcu, J.Magn. Magn. Mater. 197 (1998) 53.

[8] H. Zaman, A. Yamada, H. Fukud ,Y. Ueda, J. Electrochem. Soc. 145 (1998) 565.

[9] P E. Brandley , D. Landlot, Electrochim. Acta 45 (1999) 1077.

[10] K. Miazaki, S . Kainuma, K. Hisatake, KT. Watanabe , N. Fukumuro, ibid. 44(1999) (21/22) 3713.

[11] SH. Ge, HH. Li, C. Li, L. Xi, W. Li, J. Chi, J. Phys.: Condens. Matter 12 (2000) 5905.

[12] GR. Pattanaik, SC. Kashyap, DK. Pandya, J. Magn. Magn. Mater. 219 (2000) 309.

[13] E. G'omez, A. Laberta, A. Llorente, E. Valléz, J. Electroanal. Chem. 517 (2001) 63.

[14] R. L´opez, J. Herreros, A. Gar'cia-arribasAR, JM. Barandiar'an, ML. Fdez-gubieda, J.Magn. Magn. Mater. 196 (1999) 53.

[15] JM. Doughton, J. Magn. Magn. Mater. 192(1999)334 __

[16] C P O. Treutler, Sens. Actuators, A, 9, 2 (200).

[17] GL. Zhou, MH. Yang,CP . Flynn, Phys. Rev. Lett. 77 (1996) 4580.

[18] PE. Brandly, D. Landlot, Electrochim. Acta 45 (1999) 1077.

[19] K. Miyazaki, S. Kainuma, K. Hisatake, T. Watanabe, N. Fukumuro, Electrochim Acta 44 (1999) 3713. [20] E. Gómez, A. Laberta, A. Llorente, E. Valléz, J. Electroanal. Chem. 517 (2001) 63.

[21] I. Bakonyi, ET. Kadar, J. Toth, LF. Kiss, L. Pogany, A. Cziraki, C. Ulhaq-Bouillet, V. Pierron-Bohnes, A. Dinia, B. Arnold, K. Wetzig. Europhysics. Letters 58 (2002) 408.

[22] I. Bakonyi, E. Toth-Kadar, A. Cziraki, J. Toth, LF. Kiss, C. Ulhaq-Bouillet, V. Pierron-Bohnes, A. Dinia, B. Arnold, K. Wetzig, P. Santiago, MJ. Yacaman. J. Electrochem. Soc. 149 (2002) 469.

[23] GR. Pattanaik, SC. Kashyap, DK. Pandya, J. Electrochem. Soc. 149 (2002) C363.

[24] JJ. Kelly, P. Kern, D. Landot, J. Electrochem. Soc. 147 (2002) 3725.

[25] R. López Antón, ML. Fdez-Gubieda, A. García-Arribas, J. Herreros, M. Insausti, Materials Science and Engineering A335 (2002) 94.

[26] T. Cohen-Hyams, WD. Kaplan, D.Aurbach, YS . Cohen, J. Yahalom, J. Electrochem. Soc. 150 (2003) C28.

[27] I. Bakonyi, J. Toth, LF. Kiss, E. Toth-Kadar, L. Peter, A. Dinia, J. Magn. Magn. Mater. 269 (2004) 156.

[28] M. R. Khelladi, L. Mentar, A. Azizi, M. Boubatra, A. Kahoul, Mater Chem Phys, 122 (2010) 449.

[29] M.R. Khelladi, L. Mentar, A. Azizi, A. Sahari, A. Kahoul, Mater Chem Phys 115 (2009) 385.

[30] Gu.M, Trans Inst Metal Finish 84 (2006) 4.

[31] S Fletcher,Electrochim Acta 28(1983) 917.

[32] E. Gomez, A. Labarta, A. Lorente, E. Valles, J. Electrochem. Soc. 151 (11) (2004) C731.

[33] G. Gunawardena, G. Hills, T. Montenegro,B. Scharifker, J. Electroanal. Chem. 138 (1982) 225.

[34] B. Scharifker, G. Hills, Electrochim. Acta 28 (1983) 879.

[35] A. Maeda, M. Kume, S. Oikawa, Y. Shimizu and M. Doi, J. Phys. (1993), p. 4641.

[36] TB, Massalski, Binary Alloy Phase Diagrams, ASM International, Materials Park, OH (1990).

[37] JW. Dini, Electrodeposition, p. 156; Noyes Publications, Park Ridge, NJ (1993).

[38] T. Cohen-Hyams, WD. Kaplan, J. Yahalom, Electrochem. Solid-State Lett., 5 (2002) C75.

[39] P. Nallet, E. Chassaing, MG. Walls, MJ. Hytch, J. Appl. Phys., 79 (1996) 6884.

[40] H. Safranek, "the Properties of Electrodeposited Metals and Alloys", New York (1991), p 63.

[41] L. Péter, A. Cziráki, L. Pogány, Z. Kupay,I. Bakonyi, M. Uhlemann,M. Herrich, B. Arnold, T. Bauer, K. Wetzig, J. Electrochem. Soc. 148 (2001) C168.

[42] BD. Cullity, Elements of X-ray Diffraction, vol. 91, 2nd Ed., Addison-Wesley, Reading, MA, 1978, 501.